Internal structure of dendrimers in the melt under shear: A molecular dynamics study

Jaroslaw T. Bosko, B. D. Todd,[a] and Richard J. Sadus[b]
Centre for Molecular Simulation, Swinburne University of Technology, Hawthorn, Victoria 3122, Australia

(Received 13 February 2004; accepted 2 April 2004)

The molecular structure of fluids composed of dendrimers of different generations is studied using nonequilibrium molecular dynamics (NEMD). NEMD results for dendrimer melts undergoing planar Couette flow are reported and analyzed with particular attention paid to the shear-induced changes in the internal structure of dendrimers. The radii of gyration, pair distribution functions and the fractal dimensionality of the dendrimers are determined at different strain rates. The location of the terminal groups is analyzed and found to be uniformly distributed throughout the space occupied by the molecules. The fractal dimension as a function of strain rate displays crossover behavior analogous to the Newtonian/non-Newtonian transition of shear viscosity. © *2004 American Institute of Physics.* [DOI: 10.1063/1.1755659]

I. INTRODUCTION

Dendrimers represent a special class of highly branched synthetic polymer. They are composed of relatively short chains with multifunctional groups at both ends built around a central core with one layer added per generation. Their structure is characterized by the number of generations (g), functionality of the end groups (f), and the number of monomers in the chain units (b). Dendrimers of generation 1 to 4 with 3-functional end groups and $b=2$ are presented in Fig. 1. Generation 0 molecules (not illustrated) represent the limiting case of a simple star polymer with a central core and f linear arms. It is evident from Fig. 1 that increasing the generation number results in a highly symmetrical three-dimensional structure. The total number of monomers N grows exponentially with generation:

$$N=fb((f-1)^{g+1}-1)/(f-2)+1. \tag{1}$$

This rate of growth is faster than the available volume ($\sim g^3$) and the resulting effect of increasing density and excluded volume are responsible for unusual solution and bulk properties.[1–3]

The first theoretical analysis of the structure of dendrimers was reported by de Gennes and Hervet[4] using a mean field approach (modified version of Edwards' self-consistent fields). Assuming that the branches of growing dendrimers always face outwards and the monomers belonging to the same generation lay in concentric shells, they observed molecules with hollow flexible inner cores and dense rigid outer shells. Their work determined the limiting generation numbers for perfect growth (excluded volume effect), and distribution of terminal groups on the outermost surface. They reported that the size of dendrimers changes with the number of monomers as $R\propto N^{1/5}$, where R is the mean molecular radius of gyration, giving a fractal dimensionality $d_f=5$.

Atomistic simulations using a self-avoiding walk were reported by Lescanec and Muthukumar.[5] Molecular dynamics simulations were performed by Murat and Grest[6] and de Gennes's model was revised by Zook and Pickett.[7] Other equilibrium molecular simulation studies have reported the structure of isolated[8,9] and bulk[10] homogeneous dendritic polymers. In contrast to the early work of de Gennes and Harvet,[4] the current consensus is that the structure of dendrimers is characterized by a dense core, highly folded branches and terminal groups distributed uniformly throughout the interior of the molecule. Although there is now consistent agreement for the qualitative structural features of dendrimers, there are considerable quantitative differences which depend on the details of the dendrimer studied and the external physical conditions. The quantitative difference between different dendrimers is apparent in the scaling behavior of the radius of gyration (dendrimer size) with respect to the number of monomers. For example, the radius of gyration has been observed to scale as $N^{0.22}$ (Ref. 5), $N^{0.3}$ (Ref. 6), or $N^{3/5}$ (Ref. 7).

Theoretical models have been developed to describe the properties of dendrimers,[11] however previous work has almost exclusively described properties in solution. Relatively little theoretical or experimental work has been undertaken for either dendrimer melts or systems away from equilibrium. In contrast, this work is devoted to molecular simulations of dendrimers in the melt. We report atomistic simulations of shear-induced changes in the structure of model dendrimers using nonequilibrium molecular dynamics (NEMD). To the best of our knowledge this is the first reported NEMD study of dendrimers. However, other workers[12] have recently examined the shearing behavior of dendrimers using Brownian dynamics. In contrast to our work, these studies were confined to behavior in solution rather than a melt.

The results of our NEMD simulations in the melt indicate that at certain strain rates the molecules become stretched with fewer entangled branches. This flow-induced deformation leads to the characteristic shear-dependent vis-

[a]Electronic mail: btodd@swin.edu.au
[b]Electronic mail: rsadus@swin.edu.au

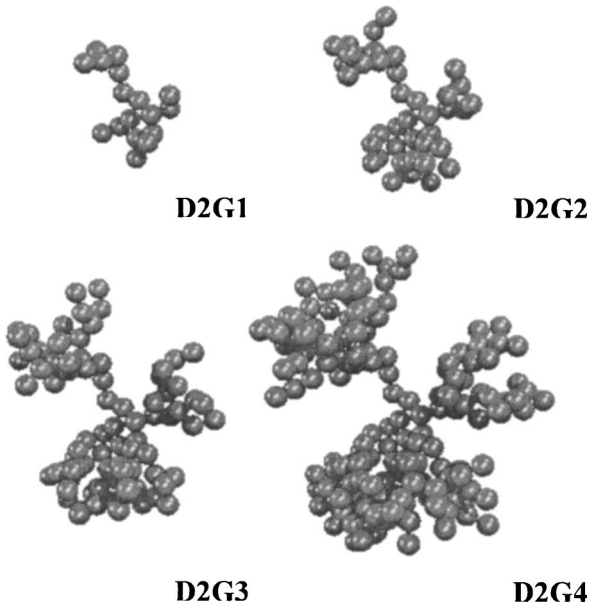

FIG. 1. Illustration of dendrimers of generations 1 to 4 modelled using freely jointed beads interacting via the FENE potential.

cosity for molecular fluids. We also calculate the fractal dimension of dendrimers and report the manner in which it changes with the strain rate. In contrast to other studies[1,5] in which a single scaling behavior for dendrimers was assumed, we attempt to analyze in detail the variation of dimensionality of dendrimers with generation number.

II. SIMULATION DETAILS

A. Dendrimer model

We model three-dimensional dendrimers at a coarse-grained level using uniform beads to construct a molecule. The freely jointed interacting beads correspond to the whole monomers or even groups of them, neglecting their atomic-scale structure. This is a reasonable assumption as we are primarily interested in the mechanical and structural properties of the macromolecules which are dominated by their large-scale properties.[13] All beads have mass assigned to $m=1$ in reduced units. The dendrimers studied here have a single core, which is the common origin of all the branches of the molecule. Examples of dendrimers composed in this way are illustrated in Fig. 1.

The component beads interact via a Weeks–Chandler–Anderson (WCA)[14] potential. The WCA potential is the Lennard-Jones potential truncated at the position of the minimum and shifted to eliminate the discontinuity:

$$U_{ij}^{\mathrm{LJ}}=4\varepsilon\left[\left(\frac{\sigma}{r_{ij}}\right)^{12}-\left(\frac{\sigma}{r_{ij}}\right)^{6}\right]+\varepsilon \quad \text{for } r_{ij}/\sigma<2^{1/6},$$
$$U_{ij}^{\mathrm{LJ}}=0 \quad \text{for } r_{ij}/\sigma\geqslant 2^{1/6}, \tag{2}$$

where r_{ij} is the separation between the sites represented by atoms i and j, ε is the potential well depth and σ is the effective diameter of the atoms. The WCA potential results in a purely repulsive potential that includes the effect of excluded volume.

Adopting the common practice of molecular simulation,[15] all quantities are reported in reduced units relative to the LJ parameters: $r_{ij}^{*}=r_{ij}/\sigma$, $\rho^{*}=\rho\sigma^{3}$, $T^{*}=k_BT/\varepsilon$, $\mathbf{P}^{*}=\mathbf{P}\sigma^{3}/\varepsilon$, $\dot{\gamma}^{*}=(m\sigma^{2}/\varepsilon)^{1/2}\dot{\gamma}$, $\eta^{*}=(\sigma^{4}/m\varepsilon)^{1/2}\eta$ with both ε and σ being assigned a value of one. Here ρ is the system density, T is the kinetic temperature, $\mathbf{P}$ is the pressure tensor, $\dot{\gamma}$ is the strain rate and η is the shear viscosity. For simplicity of notation, hereafter the asterisk will be omitted.

For the chemically bonded atoms, an attractive finitely extensible nonlinear elastic (FENE) potential[16] is added

$$U_{ij}^{\mathrm{FENE}}=-0.5kR_0^{2}\ln[1-(r_{ij}/R_0)^{2}] \quad \text{for } r_{ij}\leqslant R_0,$$
$$U_{ij}^{\mathrm{FENE}}=\infty \quad \text{for } r_{ij}\geqslant R_0, \tag{3}$$

where R_0 is a finite extensibility, and k is a spring constant. The FENE potential in combination with the WCA repulsive interaction creates a potential well for the flexible bonds that maintain the topology of the molecules. In this work we set $R_0=1.5$ and $k=30$. This means that the average distance between the connected atoms in equilibrium at temperature $T=1.25$ is approximately 0.97. The choice of intermolecular potentials for the simulation of fluids is discussed elsewhere.[15]

Collections of dendrimers with trifunctional end groups ($f=3$), spacers composed of two beads ($b=2$), and generations 1–4 (D2G1, D2G2, D2G3, D2G4) were constructed and compressed to the required density ($\rho=0.84$). The sample consisted of 256 molecules in the case of D2G1 and 125 molecules for higher generations with 19, 43, 91, and 187 beads per molecule for generations 1 to 4, respectively. Periodic boundary conditions have been applied to exclude effects associated with surfaces and the small volume of the system.

B. NEMD simulation

Shear flow of the fluid was imposed by applying a molecular version of the homogeneous isothermal shear algorithm (SLLOD).[17] The equations of motion for bead α in molecule i are given as

$$\dot{\mathbf{r}}_{i\alpha}=\frac{\mathbf{p}_{i\alpha}}{m_{i\alpha}}+\mathbf{i}\dot{\gamma}y_i,$$
$$\dot{\mathbf{p}}_{i\alpha}=\mathbf{F}_{i\alpha}-\mathbf{i}\frac{m_{i\alpha}}{M_i}\dot{\gamma}p_{yi}-\zeta^{M}\frac{m_{i\alpha}}{M_i}\mathbf{p}_i, \tag{4}$$

where $\mathbf{r}_{i\alpha}$ and $\mathbf{p}_{i\alpha}$ represent the atomic position and thermal (peculiar) momentum of site α on molecule i, $\mathbf{p}_i$ is the momentum of the molecular center of mass of molecule i and M_i is the mass of molecule i. The strain rate is defined by $\dot{\gamma}=\partial u_x/\partial y$, where $\mathbf{u}$ is the fluid streaming velocity. The streaming velocity of the molecule is determined by the position of its center of mass and has the form $\mathbf{i}\dot{\gamma}y_i$, where y_i is the position of the molecular center of mass; no further assumptions are made on the rotational degrees of freedom of the molecule. ζ^{M} is a thermostat constraint multiplier, given by

$$\zeta^M = \frac{\Sigma_{i=1}^{N_m}(\mathbf{F}_i \cdot \mathbf{p}_i - \dot{\gamma} p_{xi} p_{yi})/M_i}{\Sigma_{i=1}^{N_m} \mathbf{p}_i^2 / M_i}, \tag{5}$$

where N_m is the number of molecules in the system. To control temperature we used Gauss' principle of least constraint applied to the molecular kinetic temperature T_M calculated from the center of mass peculiar momenta according to the formula

$$\sum_{i=1}^{N_m} \frac{\mathbf{p}_i \cdot \mathbf{p}_i}{2M_i} = \frac{3N-4}{2} k_B T_M . \tag{6}$$

The algorithm has been discussed in detail previously by Edberg *et al.*[18] and has recently been used to study the nonlinear shear and elongational rheology of polymer melts.[19] The justification for using the molecular version of the SLLOD algorithm with a thermostatted molecular kinetic temperature has been discussed in detail by Travis *et al.*[20]

All simulations were performed at constant volume at a temperature $T_M = 1.25$. The equations of motion of the atoms were integrated with a time-step $\Delta t = 0.001$ (reduced units) using a fifth-order Gear predictor corrector differential equation solver.[21] After initial equilibration (typically several million time-steps depending on the strain rate) trajectories were accumulated and thermodynamic, mechanical and configurational averages were calculated.

The molecular pressure tensor can be computed as[18]

$$\mathbf{P}^M V = \sum_{i=1}^{N_m} \frac{\mathbf{p}_i \mathbf{p}_i}{M_i} - \frac{1}{2} \sum_{i=1}^{N_m} \sum_{\alpha=1}^{n} \sum_{j \neq i}^{N_m} \sum_{\beta=1}^{n} \mathbf{r}_{ij} \mathbf{F}_{i\alpha j\beta}, \tag{7}$$

where $\mathbf{r}_{ij}$ is the center of mass separation of molecules i and j, $\mathbf{F}_{i\alpha j\beta}$ is the force on site α in molecule i due to site β in molecule j, and n is the total number of interaction sites in a molecule. The strain rate dependent viscosity can by derived as

$$\eta(\dot{\gamma}) = -\frac{\langle P_{xy}^M + P_{yx}^M \rangle}{2\dot{\gamma}}. \tag{8}$$

C. Structural analysis

The extension of a molecule in space can be characterized by its radius of gyration. The average squared radius of gyration tensor is given by the expression:

$$\mathbf{R}_\mathbf{g}^2 \equiv \left\langle \frac{\Sigma_{\alpha=0}^{n} m_\alpha (\mathbf{r}_\alpha - \mathbf{g})(\mathbf{r}_\alpha - \mathbf{g})}{\Sigma_{\alpha=0}^{n} m_\alpha} \right\rangle, \tag{9}$$

where $\mathbf{g}$ is the position of the molecular center of mass, and $\langle \cdots \rangle$ denotes an ensemble average. The value of the squared radius of gyration is defined as the trace of the tensor ($R_g^2 = \mathrm{Tr}(\mathbf{R}_\mathbf{g}^2)$), which can be compared with experimentally measured radial sizes of the dendrimers.

Further analysis of the tensor of gyration can provide insights into the shape of the molecules. For each dendrimer we derived eigenvalues of the tensor of gyration (L_1, L_2, and L_3) and averaged them over the ensemble. These eigenvalues can be interpreted as the linear dimensions of the ellipsoid occupied by the average molecule discarding its orientation. At equilibrium, ratios of these eigenvalues depend on the generation of the dendrimer and converge to 1 for highest generations (spherical symmetry). Changes in these values with strain rate quantitatively describe flow induced stretching of dendrimers and this process, in combination with molecular alignment, can lead to the macroscopic anisotropy of the material. Alternatively, the tensor of gyration can be averaged over the ensemble prior to its orthogonalization. At equilibrium, because of orientational disorder, the eigenvalues (L_1', L_2', and L_3') are equal. Breaking of the spherical symmetry is associated with alignment of the dendrimers and can be directly related to birefringence experiments.

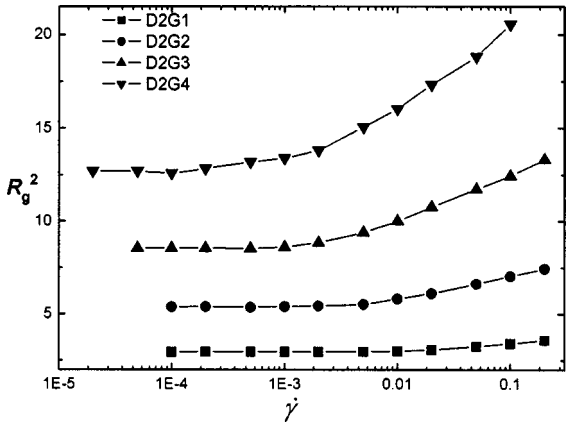

FIG. 2. Squared average radii of gyration vs strain rate for dendrimers of generations 1 to 4. Error bars have been omitted because they are smaller than the symbols representing data points.

To analyze the entanglement and back folding of the branches constituting the same dendrimer, we used a radial distribution function $g(r)$ of the terminal groups with reference to the central unit defined as

$$g(r) = \frac{\langle \Sigma_{i=1}^{N_m} \Sigma_\alpha \delta(|\mathbf{r}_{i\alpha} - \mathbf{r}_{i1}|) \rangle}{4\pi r^2 N_m}, \tag{10}$$

where $\mathbf{r}_{i1}$ is the position of the core, α runs over all terminal groups of the dendrimer.

III. RESULTS AND DISCUSSION

In contrast to previous simulation studies, which have focused on dendrimers in solution, our work was performed at conditions ($T = 1.25$, $\rho = 0.84$) that result in a melt. The structure of dendrimers in the melt away from equilibrium has been analyzed over a wide range of strain rates. The average squared radii of gyration (R_g^2) for the first four generations are shown in Fig. 2. Values of R_g^2 are a measure of the size of the dendrimer. In each case, for small strain rates (different ranges dependent on the generation), the size of the dendrimer remains constant and it is largely unchanged from its equilibrium value. In contrast for large values of strain rate, there is a noticeable increase in the value of R_g^2 which indicates that shear-induced stretching of the molecules has occurred. For a given value of strain rate, the extent of shear-induced stretching increases with generation number. For each generation the radius of gyration asymptotically follows the power law $R_g \propto \dot{\gamma}^\alpha$ with the values of the exponent α

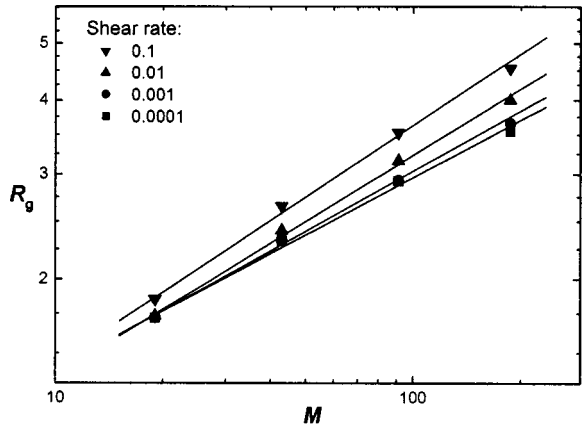

FIG. 3. The radius of gyration as a function of the molecular mass for dendrimers of generations 1 to 4 for different values of strain rate.

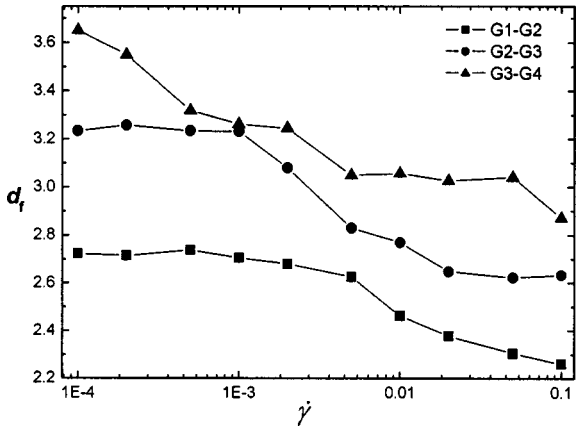

FIG. 5. The fractal dimension of dendrimers of different generations as a function of strain rate. The lines are only intended to guide the eye.

$=0.0337\pm0.0008$, $0.040\,66\pm0.0008$, 0.0472 ± 0.0006, 0.0503 ± 0.0012 for generations 1 to 4, respectively.

Radii of gyration for selected values of strain rate are shown as a function of molecular mass in Fig. 3. For each steady state condition, the slope of a linear fit was obtained. The reciprocal of this slope defines the average fractal dimension of the dendrimers: $R_g \propto M^v$, $d_f = 1/v$. For each strain rate the slope decreases with the mass, hence the fractal dimension of dendrimers increases with the generations. This is in agreement with the trends reported graphically by Stechemesser and Eimer[1] and Lescanec and Muthukumar.[5] It should be noted that using a linear fit is an approximation only. A closer examination of Fig. 3 shows that the relationship between the radius of gyration and molecular mass is not strictly linear.

The variation of the fractal dimension with respect to strain rate is illustrated in Fig. 4. The average fractal dimension of the dendrimers in equilibrium and for small strain rates is approximately 3.16 ± 0.16 and decreases with increasing strain rate down to $\sim 2.55\pm0.10$ for $\dot{\gamma}=0.1$. The equilibrium result of 3.16 is close to the fractal dimension of ~ 3 obtained by Murat and Grest[6] and observed experimentally by Scherrenberg *et al.*[2] and Stechemesser and Eimer.[1] The fact that the value of the fractal dimension is comparable to the dimensionality of the available space indicates that the structure of dendrimers is very compact.

To analyze the changes of the slope of R_g versus M with different generations, the fractal dimensions obtained from two points at a time (two generations) are illustrated in Fig. 5. The fractal dimension remains constant for small strain rates. However, at a sufficiently large value of strain rate it suddenly becomes strain rate dependent, decreasing with increasing strain rate. The crossover point from strain rate independent to strain rate dependent behavior is a function of the generation number. The crossover point shifts towards smaller values of strain rate for higher generations. For the highest generations illustrated in Fig. 5 (G3–G4), the crossover point is probably below the range of strain rates studied.

We observe that the strain rate dependence of fractal dimension (Fig. 5) is qualitatively similar to the behavior of shear viscosity. The shear viscosities of polymeric fluids exhibit a transition from Newtonian to non-Newtonian behavior.[19] At low strain rates, the viscosity is independent of strain rate, whereas at higher strain rates shear thinning is observed, i.e., the viscosity decreases as a function of strain rate. In Fig. 6 the shear viscosity of the first four generations of dendrimers is presented which demonstrate the crossover

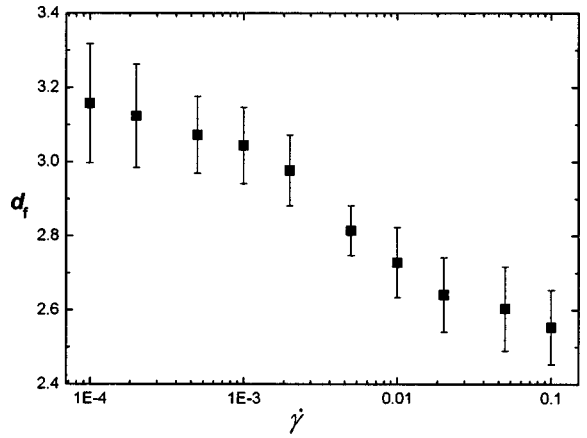

FIG. 4. The average (total) fractal dimension of dendrimers as a function of strain rate.

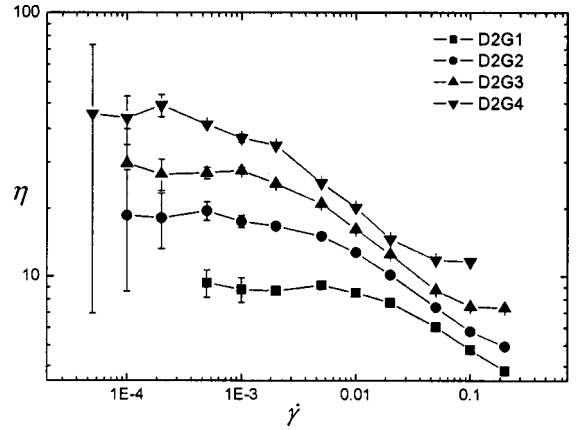

FIG. 6. The viscosity-strain rate behavior for dendrimers of generations 1 to 4. The lines are only intended to guide the eye.

from Newtonian to non-Newtonian behavior. The crossover values of strain rate for the viscosity and fractal dimension phenomena cannot be compared directly. The viscosity-strain rate curves characterize the behavior for a given dendrimer generation, whereas fractal dimensions were derived from the changes between the generations. However, comparison of Fig. 5 with Fig. 6 shows that there is at least qualitative agreement in terms of the relative position of the crossover points. The rheological properties of dendrimer melts will be discussed in more detail in a forthcoming publication.[22]

The fractal dimensions in equilibrium ($\dot{\gamma}=0$) can be directly compared with the values measured experimentally by Mallamace *et al.*[3] They report the fractal dimension of the low generation dendrimers as $d_f \approx 2.4 \pm 0.4$. Our value of 2.7 is in good agreement with their experimental results. For higher generations, the fractal dimension gradually increases through 3.2 in the middle range to 3.7 for the largest dendrimer.

To analyze flow-induced changes on the shape of dendrimers in greater detail, we derived the eigenvalues of the tensor of gyration. In Fig. 7 we present the averaged eigenvalues of the tensor as well as the eigenvalues of the averaged tensor of gyration for the dendrimers of generation 3 (results for other generations are qualitatively similar). The variation of the former can be related to the stretching of the molecules and becomes significant at the strain rates above the critical value discussed above. This is different in the case of the eigenvalues of the averaged tensor of gyration, which also take into account the orientation of the molecules. These values depart from the equilibrium values starting from the smallest values of the strain rate. Direct comparison of the behavior of these properties with the variation of viscosity with respect to strain rate [Fig. 7(c)] indicates that the onset of flow-induced molecular deformation occurs at approximately the same strain rate at which the crossover from Newtonian to non-Newtonian regimes is observed. This suggests that deformation of dendrimers is mainly responsible for the viscoelastic properties of the melt. Molecular alignment, which occurs at all strain rates, appears to have a less significant influence than deformation.

Figure 8(a) shows the distribution of the terminal monomers from the center of the molecule at a weak field strength close to equilibrium. In Fig. 8(b) the same curves are shown for a system away from equilibrium at a strain rate $\dot{\gamma}=0.1$, and in Fig. 8(c) we give a comparison of distributions at both field strengths for a D2G4 dendrimer. In each case the end groups are found everywhere throughout the interior of the molecule. Our finding is in agreement with earlier computer simulations[5–7,9] and the experimentally observed back folding of branches by Scherrenberg *et al.*[2]

When the system undergoes shearing flow, the dendrimers become stretched (see radii of gyration), as does the distribution of the monomers constituting the outmost shell. The fact that some of them are found at the distance of $(g+1)P\bar{l}$ (g = generation number, $P=2-$ length of the linear units between the branching points, $\bar{l}$ = average bond length) indicates that some of the branches are fully stretched.

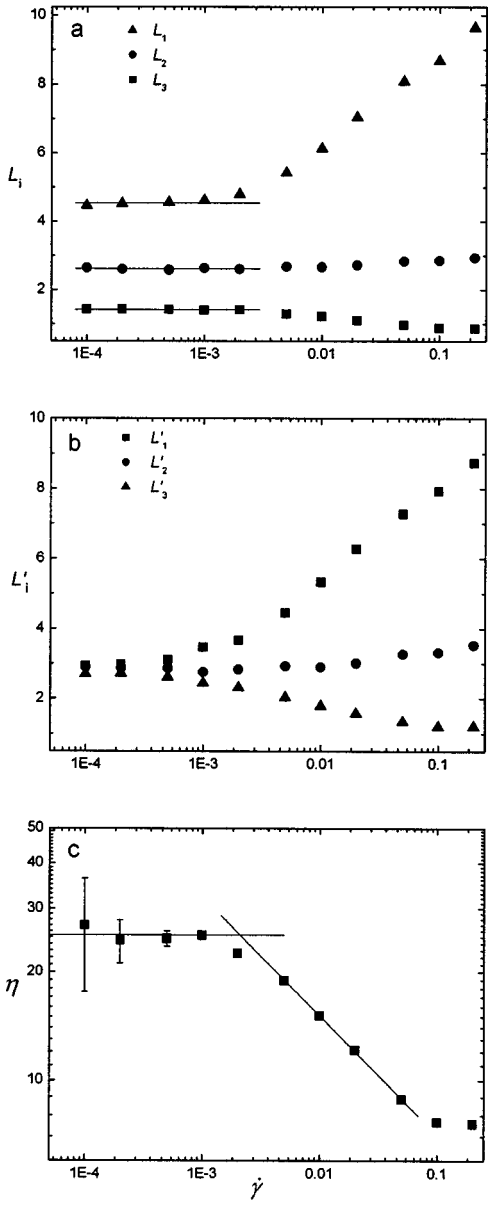

FIG. 7. The averaged eigenvalues of the molecular tensor of gyration (a), eigenvalues of averaged tensor of gyration (b), and the shear viscosity (c) as a function of strain rate for the dendrimer of generation 3 (D2G3). In panel (a), the lines represent fits of L_i in the range of small strain rates, whereas in panel (c) the Newtonian viscosity and a power-law function for the non-Newtonian viscosity were fit.

IV. CONCLUSIONS

For the first time, NEMD simulations are reported for the shearing behavior of dendrimers in the melt of generations up to four. The variation of viscosity as a function of strain-rate displays the characteristic transition from Newtonian to non-Newtonian behavior that is common to many real macromolecules. We observe that the variation of the fractal dimension with respect to strain rate behaves in an analogous way to shear viscosity with a crossover point between strain rate independent and strain rate dependent regions. The fractal dimension has values from 2.4–3.7 depending on the strain rate. The values obtained close to equilibrium are consistent with experimental equilibrium values. Analysis of the radius of gyration shows that shear induced stretching occurs

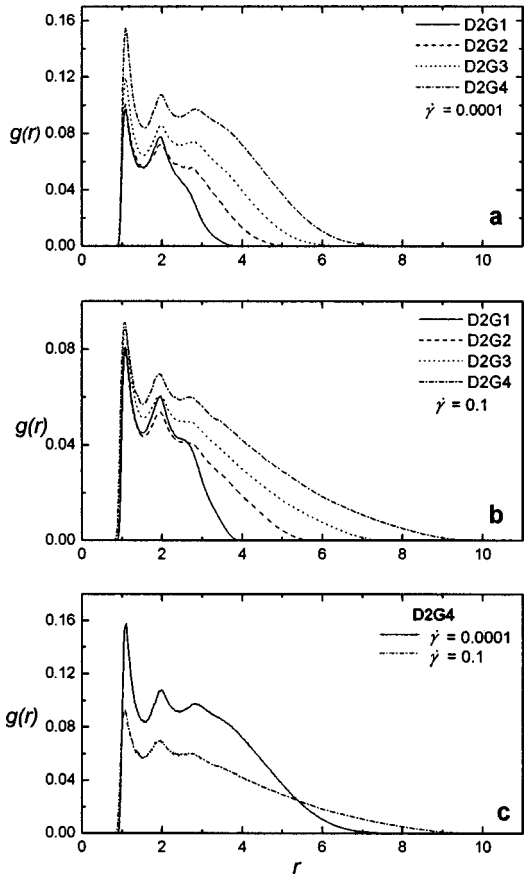

FIG. 8. Distribution of the terminal groups from the central (core) unit at (a) close to equilibrium ($\dot{\gamma}=0.0001$) and (b) $\dot{\gamma}=0.1$. A comparison of close to equilibrium and non-equilibrium results for the D2G4 dendrimer is illustrated in (c).

and this effect is particularly pronounced for large dendrimers. The deformation of molecular shape is mainly responsible for the macroscopically observed shear thinning of the dendrimer melt. The onset of both shape deformation and shear thinning occur at a specific value of strain rate, which depends on the generation of the dendrimer. In contrast, the concurrent process of molecular alignment is observed for the whole range of strain rates. Values of the radial distribution functions indicate that the terminal end groups can be located in the interior of the dendrimer which is consistent with experimentally observed back folding of branches.

ACKNOWLEDGMENTS

The authors thank the Australian Research Council for supporting this work as a Discovery Project. The Australian Partnership for Advanced Computing provided a generous allocation of computing time. The work has also benefited from discussions with Dr. Leo Lue (UMIST). One of the authors (J.T.B.) thanks the Gdansk University of Technology for encouraging his participation in this work.

[1] S. Stechemesser and W. Eimer, Macromolecules **30**, 2204 (1997).
[2] R. Scherrenberg, B. Coussens, P. van Vliet, G. Edouard, J. Brackman, and E. de Brabander, Macromolecules **31**, 456 (1998).
[3] F. Mallamace, E. Canetta, D. Lombardo, A. Mazzagalia, A. Romeo, L. M. Scolaro, and G. Maino, Physica A **304**, 235 (2002).
[4] P. G. de Gennes and H. Hervet, J. Phys. (France) Lett. **44**, L351 (1983).
[5] R. L. Lescanec and M. Muthukumar, Macromolecules **23**, 2280 (1990).
[6] M. Murat and G. S. Grest, Macromolecules **29**, 1278 (1996).
[7] T. C. Zook and G. T. Pickett, Phys. Rev. Lett. **90**, 015502 (2003).
[8] A. M. Naylor, W. A. Goddard III, G. E. Kiefer, and D. A. Tomalia, J. Am. Chem. Soc. **111**, 2239 (1989); M. L. Mansfield and L. I. Klushin, Macromolecules **26**, 4262 (1993); M. L. Mansfield and M. Jeong, *ibid.* **35**, 9794 (2002); Z. Y. Chen and S.-M. Gui, *ibid.* **29**, 7943 (1996); L. Lue and J. M. Prausnitz, *ibid.* **30**, 6650 (1997).
[9] E. G. Timoshenko, Y. A. Kuznetsov, and R. Connolly, J. Chem. Phys. **117**, 9050 (2002).
[10] L. Lue, Macromolecules **33**, 2266 (2000); N. Zacharopoulos and I. G. Economou, *ibid.* **35**, 1814 (2002).
[11] R. La Ferla, J. Chem. Phys. **106**, 688 (1997); F. Ganazzoli, R. La Ferla, and G. Raffaini, Macromolecules **34**, 4222 (2001).
[12] A. V. Lyulin, G. R. Davies, and D. B. Adolf, Macromolecules **33**, 6899 (2000); **33**, 3294 (2000); A. V. Lyulin, D. B. Adolf, and G. R. Davies, *ibid.* **34**, 3783 (2001); P. F. Sheridan, D. B. Adolf, A. V. Lyulin, I. Neelov, and G. R. Davies, J. Chem. Phys. **117**, 7802 (2002).
[13] M. Doi and S. F. Edwards, *The Theory of Polymer Dynamics* (Clarendon, Oxford, 1987).
[14] J. D. Weeks, D. Chandler, and H. C. Anderson, J. Chem. Phys. **54**, 5237 (1971).
[15] R. J. Sadus, *Molecular Simulation of Fluids: Algorithms and Object-Orientation* (Elsevier, Amsterdam, 1999).
[16] H. R. Warner, Jr., Ind. Eng. Chem. Fundam. **11**, 379 (1972); G. S. Grest and K. Kremer, Phys. Rev. A **33**, 3628 (1986).
[17] D. J. Evans and G. P. Morriss, *Statistical Mechanics of Nonequilibrium Liquids* (Academic, London, 1990).
[18] R. Edberg, D. J. Evans, and G. P. Morriss, J. Chem. Phys. **84**, 6933 (1986).
[19] P. J. Daivis, M. L. Matin, and B. D. Todd, J. Non-Newtonian Fluid Mech. **111**, 1 (2003).
[20] K. P. Travis, P. J. Daivis, and D. J. Evans, J. Chem. Phys. **103**, 1109 (1995).
[21] C. W. Gear, *Numerical Initial Value Problems in Ordinary Differential Equations* (Prentice-Hall, Englewood Cliffs, NY, 1971).
[22] J. T. Bosko, B. D. Todd, and R. J. Sadus (unpublished).